Journal of
Materials Chemistry C

Accepted Manuscript

This article can be cited before page numbers have been issued, to do this please use: Z. Li, K. Tao, J. Ma, Z. Gao, V. Koval, C. Jiang, G. Viola, H. Zhang, A. Mahajan, J. Cao, M. Cain, I. Abrahams, C. Nan, C. Jia and H. Yan, *J. Mater. Chem. C*, 2018, DOI: 10.1039/C8TC00161H.

ROYAL SOCIETY OF CHEMISTRY

rsc.li/materials-c

View Article Online
DOI: 10.1039/C8TC00161H

Journal Name

ARTICLE

$Bi_{3.25}La_{0.75}Ti_{2.5}Nb_{0.25}(Fe_{0.5}Co_{0.5})_{0.25}O_{12}$, a single phase room temperature multiferroic

Received 00th January 20xx,
Accepted 00th January 20xx

DOI: 10.1039/x0xx00000x

www.rsc.org/

Zheng Li,[a] Kun Tao,[b] Jing Ma,[c] Zhipeng Gao,[d] Vladimir Koval,[e] Changjun Jiang,[b] Giuseppe Viola,[f] Hangfeng Zhang,[g] Amit Mahajan,[a] Jun Cao,[a] Markys Cain,[h] Isaac Abrahams,[g] Cewen Nan,[c] Chenglong Jia,*[b] and Haixue Yan,*[a]

Multiferroics (MFs) have attracted great research interest due to the coexistence of ferroelectric and magnetic ordering, as well as magnetoelectric (ME) coupling. At present, there is a very limited number of single-phase MFs known and these are still far from practical applications. In single-phase MFs, the simultaneous presence of electric and magnetic dipoles does not guarantee strong (ME) coupling, as the microscopic mechanisms of ferroelectricity and magnetism are quite different and do not intrinsically interact with each other. Here we show that in the ceramic system, $Bi_{3.25}La_{0.75}Ti_{3-2x}Nb_x(Fe_{0.5}Co_{0.5})_xO_{12}$, the x = 0.25 composition is ferroelectrically and ferromagnetically active at room temperature. A single-phase structure is supported by XRD, SEM/EDX and neutron diffraction data. Clear ME couplings were observed in this single-phase material at room temperature, where the magnetic iron and cobalt ions contribute to ferroelectric polarization and magnetic moment simultaneously. The results of structural, electrical and magnetic measurements are supported by first principle calculations. This material represents one of the first truly single phase bulk ceramics that exhibits multiferroic behaviour at room temperature and its discovery will help to guide the design of room temperature single-phase MFs with strong ME coupling for sensors and solid-state memory applications.

Introduction

Multiferroic materials[1] exhibit coupling between magnetic and electric polarization and are being investigated for a number of applications including the next generation of memory devices with low energy consumption[2, 3] and energy harvesting.[4-6] Recently, ferroelectric random access memories (FRAM) have achieved fast access speed (about 5 ns) and high density (64 Mb),[7] but they are limited by the need for destructive read and reset operations. MFs offer the possibility of multistate memory with fast low-power electrical write and non-destructive magnetic read operations.[8, 9] For energy applications the strength of the magnetoelectric coupling must be high enough to allow harvesting of electrical energy through magnetic stimuli. [6]

Aside from the potential applications, the fundamental physics of MFs is rich and fascinating. At present, there are very few single-phase MFs known. This is mainly due to the fact that the conventional mechanism for cation off-centring in ferroelectrics (which requires formally empty *d*-orbitals) and the formation of magnetic moments (which usually results from partially filled *d*-orbitals) are mutually exclusive.[10] Furthermore, the possibility of practical application of the known single-phase MFs is remote, since they exhibit multiferroic properties only at very low temperatures,[1] while at room temperature the magnetoelectric coupling is weak.[11-14] Although some materials were previously reported as single-phase, secondary phases were found using SEM/EDX in subsequent studies.[15] $BiFeO_3$ is still the only well-known single-phase room temperature multiferroic material.[16] However, $BiFeO_3$ is far from application, due to its high electrical conductivity.[17] Therefore, the development of new MF materials, with better performance, is seen as a pressing need.

In single-phase multiferroics, the simultaneous presence of electric and magnetic dipoles does not guarantee strong intrinsic magnetoelectric (ME) coupling. Strong ME coefficients are expected in single-phase MFs because the same magnetic ions contribute to ferroelectric polarization and magnetic moment simultaneously.[18] Recently, Aurivillius compounds have attracted much attention with respect to multiferroic activity.[19-22] The structure of these compounds consists of bismuthate layers of general formula $(Bi_2O_2)_n^{2n+}$, separated by

[a] School of Engineering and Materials Science, Queen Mary University of London, Mile End Road, London, E1 4NS, United Kingdom, h.x.yan@qmul.ac.uk
[b] Key Laboratory for Magnetism and Magnetic Materials of MOE, Lanzhou University, Lanzhou 730000, China, cljia@lzu.edu.cn
[c] School of Materials Science and Engineering, and State Key Laboratory of New Ceramics and Fine Processing Tsinghua University Beijing 100084, China
[d] National Key Laboratory of Shock Wave and Detonation Physics, Institute of Fluid Physics China Academy of Engineering Physics Mianyang 621900, China
[e] Institute of Materials Research Slovak Academy of Sciences Watsonova 47, 04001 Kosice, Slovakia
[f] Department of Applied Science and Technology, Institute of Materials Physics and Engineering, Corso Duca degli Abruzzi 24, 10129 Torino, Italy
[g] School of Biological and Chemical Sciences Queen Mary University of London Mile End Road, London, E1 4NS, United Kingdom
[h] Electrosciences Ltd, Farnham, Surrey GU9 9QT, United Kingdom
† Footnotes relating to the title and/or authors should appear here.
Electronic Supplementary Information (ESI) available: [details of any supplementary information available should be included here]. See DOI: 10.1039/x0xx00000x

View Article Online
DOI: 10.1039/C8TC00161H

perovskite slabs of general formula $(A_{m-1}B_mO_{3m+1})^{2n-}$, where m is the number of octahedral layers in the perovskite slab.

In Aurivillius compounds, the spontaneous polarization (P_s) originates from the off-centre movement of the octahedral cations in one direction within the basal (*a*-*b*) plane.[23, 24] A variety of transition metal elements, such as Fe, Co, and Mn, can be accommodated in the B-site.[25-27] In this case, the magnetic ions in the B-site are responsible for both ferroelectricity and magnetism and hence ME coupling can be achieved.

In the present work, $Bi_{3.25}La_{0.75}Ti_3O_{12}$ (BLT), a material typically used for non-volatile ferroelectric random access memory (FRAM), because of its excellent fatigue resistance and large spontaneous polarizations along the *a*-axis,[28, 29] was selected as the base composition. A range of compositions of general formula $Bi_{3.25}La_{0.75}(Fe_{0.5}Co_{0.5})_xTi_{3-2x}Nb_xO_{12}$ (BFCT100*x*, x = 0.05, 0.25 and 0.35) was studied with Nb B-site substitution, aimed not only at maintaining electroneutrality in the presence of the magnetic ions Fe^{3+}/Co^{3+}, but also to decrease electrical conductivity.[30] In this way a single phase composition supporting the highest level of substitution by magnetic ions was identified. The existence of ME coupling at room temperature was confirmed in single phase ceramics and is supported by first principles modelling.

Experimental

Sample preparation

Samples of composition $Bi_{3.25}La_{0.75}Ti_{3-2x}Nb_x(Fe_{0.5}Co_{0.5})_xO_{12}$ (BFCT100*x*, x = 0.05, 0.25 and 0.35) were prepared from stoichiometric amounts of Bi_2O_3 (Alfa Aesar,99.975%), La_2O_3 (Sigma Aldrich, 99.9%), Fe_2O_3(Alfa Aesar 99.9%), Co_3O_4 (Sigma Aldrich, 99.9%), Nb_2O_5 (Alfa Aesar 99.9%) and TiO_2 (Alfa Aesar 99.8%). The starting mixtures were ball milled for 4 h in methylated spirits. After drying the mixtures were calcined at 900 °C for 4 h. Textured ceramics were obtained in a two-step process using spark plasma sintering (HPD 25/1 FCT, Germany). The powders were sintered at 825-850 °C for 5 min under a uniaxial pressure of 80 MPa in a graphite die, with an inner diameter of 20 mm. The dense samples were superplastically deformed at 925-950 °C for 5 min under a pressure of 50 MPa in a larger graphite die with an inner diameter of 30 mm. In order to remove carbon arising from the graphite dies, the sintered ceramics were annealed at 800 °C for 10 h in air.

Crystal structure characterization

The bulk ceramics were cut perpendicular to the SPS pressure direction. The crystal structures of the obtained ceramics were analysed at room temperature using a PANalytical X'Pert Pro diffractometer, with nickel filtered Cu Kα radiation (λ = 1.5418 Å). Data were collected in flat plate θ/θ geometry over the 2θ range 5 to 120° in steps of 0.0167° with an effective scan time of 400 s per step. Calibration was performed using an external LaB_6 standard. Powder neutron diffraction data were collected at room temperature on the BFCT25 sample using the Polaris diffractometer at the ISIS facility, Rutherford Appleton Laboratory, UK. A data set of 400 μA h was collected on a powdered sample in a 5 mm diameter vanadium can. Data for the backscattering bank (average angle 146.72°) normalized against those for a vanadium rod were used in subsequent calculations. Structure refinement was carried with the GSAS suite of programmes[31] taking the structure of $Bi_{3.75}La_{0.25}Ti_3O_{12}$ in space group *B*2*cb* as a starting model.[32] Structure diagrams were drawn using VESTA.[33] The surface morphology was studied using scanning electron microscopy (SEM) (FEI Inspect-F, Hillsboro, OR, USA).

Ferroelectric characterization: Ferroelectric *I*–*E* (current–electric field) and *P*–*E* (polarization–electric field) hysteresis loops were measured using a ferroelectric hysteresis measurement tester (NPL, UK).[34] The temperature dependencies of the relative dielectric permittivity and loss were measured at different frequencies using an LCR meter (Agilent, 4284A, USA) and a purpose-made furnace. The morphology of the ferroelectric domains was observed by Piezoresponse force microscopy (NT-MDT, Ntegra systems, Russia), using a non-magnetic conductive tip, operated at 70 kHz with a 10 V AC electric field.

Magnetization characterization

The magnetic (M-H) hysteresis loops and temperature dependence of magnetization were measured using a superconducting quantum interference device magnetometer (Quantum Design, a model MPMS (SQUID) VSM, USA) over the temperature range 1.8 K to 1000 K in the magnetic field range -1 T to 1 T. The M-T curves were corrected for a paramagnetic contribution of individual magnetic atoms with no magnetic interaction. Electron spin resonance (ESR) measurements were performed using a JEOL, JES-FA 300 (X-band at ω = 8.969 GHz with a power of 1 mW) spectrometer at room temperature. The magnetoelectric coupling coefficient was measured using a magnetoelectric measurement system (Quantum Design, Super-ME-II, USA).[35] The samples were subjected to a DC magnetic field that varied linearly with time (0 - 3 kOe). An AC magnetic field (H_{ac}) of 5.6 Oe, with a frequency of 1 kHz was superimposed onto a DC field.

First principles modelling of magnetization

First principles calculations were carried out based on density functional theory (DFT), as implemented in the Vienna ab initio simulation package (VASP), with projector augmented wave (PAW) potentials and the generalized gradient approximation (GGA) of Perdew, Burke, and Ernzerhof (PBE). The basis set contained plane waves with a kinetic energy cutoff of 500 eV and the total energy was converged to 10^{-6} eV. The geometry of the cluster was optimized with no symmetry constraints until all residual forces on each atom were less than 0.01 eV $Å^{-1}$. A 2 × 1 BLT supercell was employed in all calculations, in which two Ti atoms were substituted by the Fe/Co magnetic atoms. To improve the description of the Fe/Co 3*d* electrons, the GGA+*U* method was introduced to take the strong correlation into account. Calculations with U = 1.0-6.0 eV were performed to assess the magnetic coupling on the magnitude of Hubbard U. For BFCT25, reasonable agreement was reached once effective U = 2.0 eV and U = 3.0 eV for Fe and Co atoms, respectively.

View Article Online
DOI: 10.1039/C8TC00161H
Journal Name ARTICLE

These values for Hubbard *U* lie in the typical range that has been successfully used to describe the magnetic properties of $BiFeO_3$,[36] Aurivillius phase $Bi_5FeTi_3O_{15}$,[37] and different spin states of Co^{3+} for perovskites $LaCoO_3$.[38]

Results and discussion

Structural characterisation

The X-ray powder diffraction (XRD) data (supplementary information Figure S1) revealed that the BFCT5 and BFCT25 powders are single-phase compounds. Their diffractograms can be indexed using the orthorhombic structure of BLT (ICDD file #89-7500). The XRD pattern of the $x = 0.35$ composition showed traces of a secondary phase, $Bi_2Ti_2O_7$ (ICDD file #32-118), indicating that this composition lies above the solid solution limit. The fitted neutron diffraction data for the $x = 0.25$ composition are shown in **Figure 1**. The crystal structure and refinement parameters, refined structural parameters and significant contact distances are given as supplementary

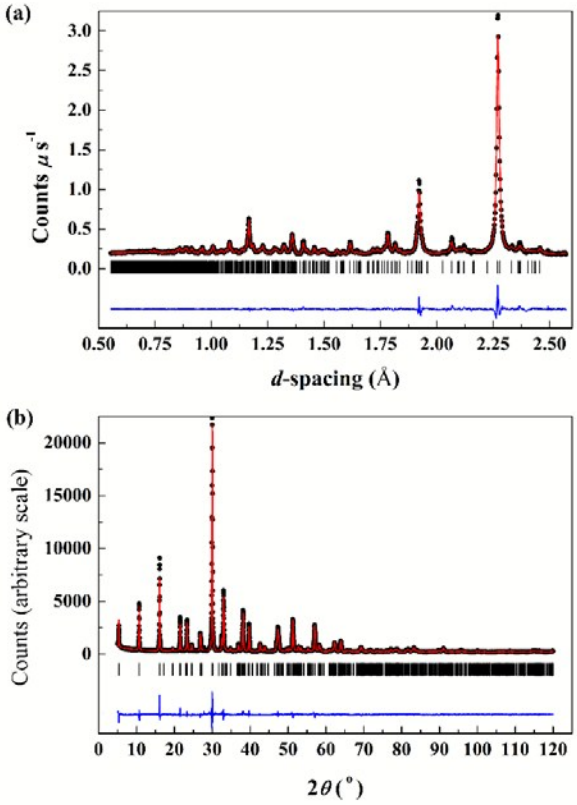

Figure 1. Fitted diffraction profiles for BFCT25 (a) neutron and (b) X-ray diffraction data; observed (black open circles), calculated (red line) and difference (blue line) patterns obtained from the Rietveld analysis. The allowed Bragg reflections for the corresponding space group B2cb are indicated by black ticks.

information in Tables S1, S2 and S3, respectively. The structure can be described as consisting of layers of bismuth oxide of general formula $[Bi_2O_2]_n^{2n+}$, separated by perovskite slabs containing three layers of corner sharing perovskite-like Ti/Nb/Fe/Co-O_6 octahedra, with Bi^{3+} and La^{3+} ions located in the A site, within these slabs (**Figure 2**). The coordination of the Bi^{3+} cations on the Bi(2) site in the bismuthate layer is essentially four pyramidal, consisting of four Bi-O bonds with an average Bi-O distance of 2.31 Å, two longer Bi-O contacts of around 2.65 Å and two at 3.10 Å. This atomic arrangement results in a distorted square antiprismatic site geometry and gives rise to the stereochemical activity of the Bi $6s^2$ lone pair of electrons. In the case of the Bi/La(1) site within the perovskite slab, there is also evidence of stereochemical activity of the bismuth lone pair. The partial occupancy of this site by La^{3+} leads to a smaller average stereochemical distortion for this site compared to the Bi(2) site. Cumby and Attfield[39] have recently proposed a novel method for examining polyhedral distortions through ellipsoidal analysis. The method allows for comparison of different size coordination polyhedra through the variance of the mean ellipsoid radius $\sigma^2(R)$, where large values indicate greater distortion and the ellipsoid shape parameter *S*, which can vary between -1 and +1, corresponding to oblate and prolate ellipsoids, respectively, with perfect spherical geometry indicated by an *S* value of zero. In the case of the Bi sites, assuming a cut off distance of 3.3 Å, Bi(1) and Bi(2) sit in 12 and 8 coordinate sites, respectively, with mean ellipsoid radii, < R >, of 2.880 Å, and 2.635 Å, variances of 0.0872 Å^2 and 0.3176 Å^2 and *S* values of 0.160 and -0.375, respectively. The larger value of $\sigma^2(R)$ for Bi(2) and the larger magnitude of its shape parameter are consistent with this site showing greater stereochemical distortion compared to the Bi(1) site and compare with the values of R = 2.627 Å, $\sigma^2(R) = 0.2876$ Å^2 and $S = 0.377$ for the analogous Bi(2) site in $Bi_2La_2Ti_3O_{12}$.[40] A number of models for the cation distribution in Aurivillius phase materials were investigated, including different A site and B site cation distributions. In the case of the A site distribution, no

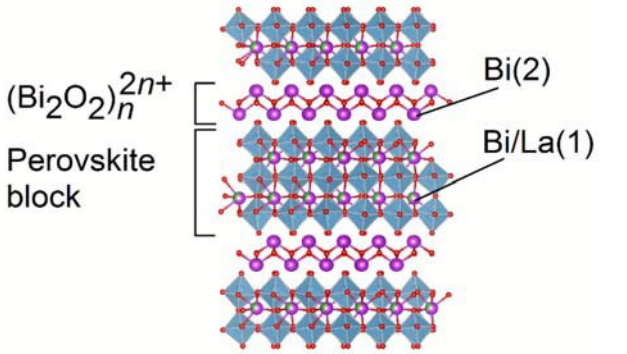

Figure 2. (1 1 0) projection of the structure of $Bi_{3.25}La_{0.75}Ti_{2.5}Nb_{0.25}Fe_{0.125}Co_{0.125}O_{12}$. The Bi and O atoms are represented by violet and red circles, respectively. A partial occupation of the perovskite A sites by La is indicated by a partial green shading. Ti/Nb/Fe/Co octahedra are shown in blue.

evidence of the presence of La^{3+} on the Bi(2) site was found. This is in contrast to the situation in heavily La-substituted compound $Bi_2La_2Ti_3O_{12}$,[40] where a degree of site sharing on both sites exists and is accompanied by a removal of the orthorhombic distortion to yield a tetragonal structure. In the case of the B site cation distribution, the best fit was obtained using an approximately even distribution of cations over the two perovskite B sites. In the final refinement, the Fe/Co ratio

View Article Online
DOI: 10.1039/C8TC00161H

was allowed to vary between these two crystallographic sites. Both octahedral sites show small prolate distortions of their ellipsoids with *S* values of 0.0193 and 0.0101 for Ti/Nb/Fe/Co(1) and Ti/Nb/Fe/Co(2), respectively, but with little variance of their mean ellipsoid radii, with respective < *R* > values of 1.953 Å and 1.980 Å and variances of 0.0015 and 0.0034.

Scanning electron microscopy was used to examine morphology of the prepared ceramics. SEM images of the BFCT5 and BFCT25 textured ceramics are shown in the supplementary material (Figure S2). Plate-like grains oriented perpendicularly to the SPS pressure direction are observed in the micrographs. The high values of the Lotgering orientation factor (f = 0.72 and 0.75 for BFCT5 and BFCT25, respectively) confirm a highly grain-oriented structure for both compositions.

Ferroelectric Properties

Figure 3a and 3b display the current-electric field (*I-E*) and polarization-electric field (*P-E*) hysteresis loops of the grain-oriented BFCT5 and BFCT25 ceramics, respectively, obtained at room temperature in a direction perpendicular to the SPS pressure direction. The occurrence of current peaks in the *I-E* loops implies ferroelectric domain switching upon electric field reversal.[41] The maximum value of the remnant polarization (P_r) decreases as the concentration of magnetic ions increases. The P_r values for BFCT5 and BFCT25 are 14.08 μC cm^{-2} and 12.43 μC cm^{-2}, respectively. Figure 3c and 3d show the temperature dependence of the relative dielectric permittivity and loss of BFCT5 and BFCT25 ceramics measured perpendicularly to the SPS pressure direction. The ferroelectric Curie points (FE T_c) of BFCT5 and BFCT25, as determined from the dielectric peak position, are 638.2 K and 556.5 K, respectively. FE T_c decreases with increasing concentration of magnetic ions. Such behaviour has been observed in other substitutionally-modified Aurivillius phase MFs and suggests the formation of a solid solution in the present system, with the trivalent Fe/Co ions replacing Ti^{4+} ions at the B-sites. A broadening of the FE T_c peaks is likely caused by the existence of local Fe/Co-rich regions in the structure and is discussed below. Based on the structural parameters given in Table S2, the value of the spontaneous polarization P_s along the *a*-axis of the ferroelectric BFCT25 was calculated using Shimakawa`s model.[42] The atomic displacements and contribution of each ion to P_s are illustrated in Figure 3e and 3f, respectively. The total P_s obtained from the model was found to be 29.9 μC cm^{-2}.

Magnetic Properties

The magnetization of BFCT5 and BFCT25 subjected to a magnetic field (H), of 200 Oe was measured using a SQUID magnetometer in the temperature range from 1.8 K to 1000 K. As illustrated in **Figure 4**a, the lightly doped BFCT5 sample shows paramagnetic behaviour, which implies a random occupancy of the B sites by magnetic ions, in the absence of long range magnetic ordering, down to 1.8 K. However, with increasing doping level, local Fe/Co rich regions emerge in BFCT25 and magnetic ordering is expected to arise from the exchange interaction between adjacent magnetic ions. By fitting the *M-T* curve of BFCT25 with the Curie-Weiss law, *i.e.* $\chi_m = C/(T - T_{cm})$, where χ_m is magnetic susceptibility, C is Curie constant and T_{cm} is magnetic Curie point, three distinct magnetic transitions at about 50 K, 160 K and 380 K are distinguished (*c.f.* Figure. 4b and Figure.5). The ferromagnetic

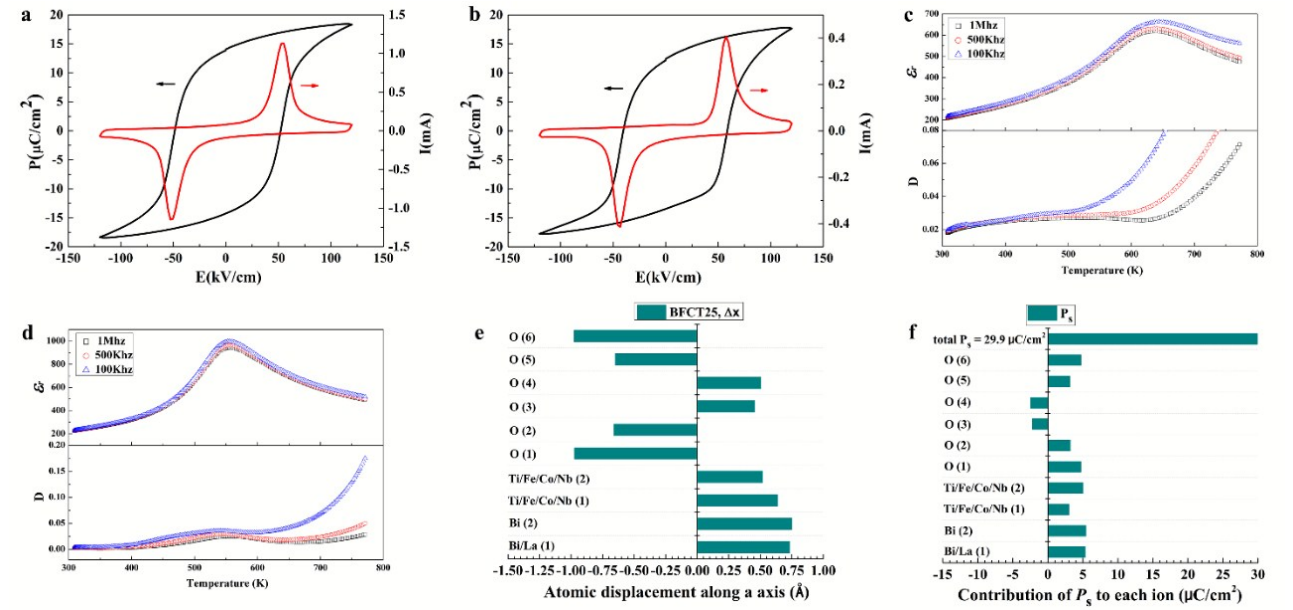

Figure 3. The P-I-E loops of (a) BFCT5 and (b) BFCT25. The temperature dependence of the relative dielectric permittivity (εr) and dielectric loss (D) of the BFCT5 and BFCT25 ceramics is shown in (c) and (d), respectively. (e) The ionic displacements and (f) the individual contributions of each ion to the total spontaneous polarization Ps in BFCT25.

View Article Online
DOI: 10.1039/C8TC00161H

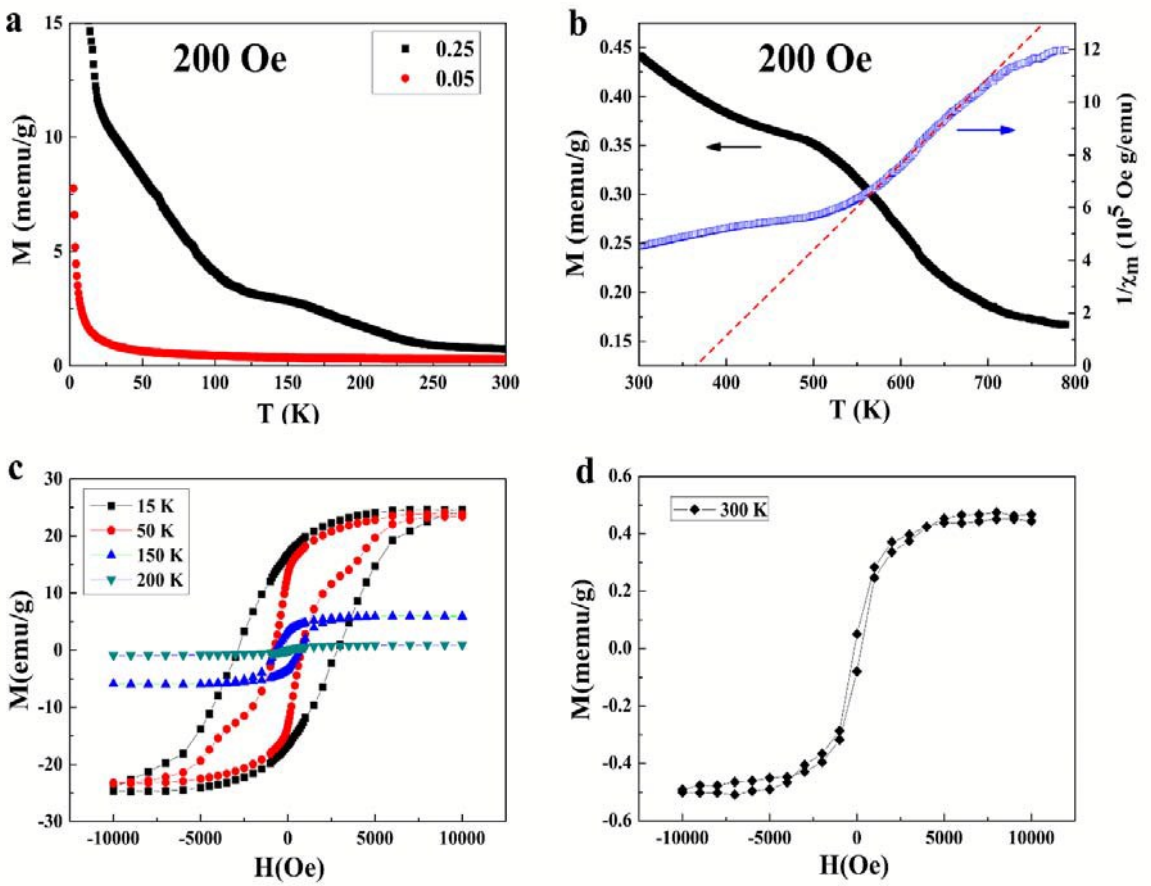

Figure 4. (a) The temperature dependence of magnetization of BFCT5 and BFCT25 ceramics (5-300 K); (b) the temperature dependence of magnetization and inverse susceptibility of BFCT25 (300-800 K); (c) and (d) the field dependence of magnetization for BFCT25 at 15 K, 50 K, 150 K, 200 K, and 300 K, respectively.

nature of the transitions is strongly supported by the magnetic hysteresis loops in Figure 4c and 4d, where the paramagnetic contribution is subtracted. The measured electron spin resonance (ESR) spectrum of BFCT25 shows a sharp ferromagnetic resonance peak at low magnetic fields and a broad paramagnetic peak at high magnetic fields (Figure S3), which confirm the ferromagnetic state of the sample. The observation of a small remnant magnetization and a rapid increase in magnetization at 300 K at low magnetic fields suggests a random distribution of Fe/Co rich regions in BFCT25, leading to a spin-glass-like behaviour at low temperatures, as shown by the zero-field-cooling (ZFC)/field-cooling (FC) experiments (Figure 6).[43]

Simulation

In order to understand the nature of the ferromagnetic properties of BFCT25, DFT calculations were performed (Table S4). The substitution positions of Fe and Co atoms for Ti atoms were determined by the total minimum energy of the Fe^{3+} and Co^{3+} ions which are connected through an O atom. This suggests Fe^{3+}-O-Fe^{3+}, Fe^{3+}-O-Co^{3+} and Co^{3+}-O-Co^{3+} magnetic interactions are possible in BFCT25. To correctly treat the exchange-correlation potential and the interaction between the Fe/Co 3*d* electrons, the GGA+*U* method was employed. Figure 7 shows an example of the exchange properties between adjacent FeO_6 and CoO_6 tilted octahedra with Hubbard *U* corrections of U_{Fe} = 2 eV and U_{Co} = 3 eV, respectively. From Figure 5b, it can be seen that the magnetism of the system mainly originates from the dopant Fe^{3+} and an intermediate-spin state of Co ions (2.604 and

View Article Online
DOI: 10.1039/C8TC00161H

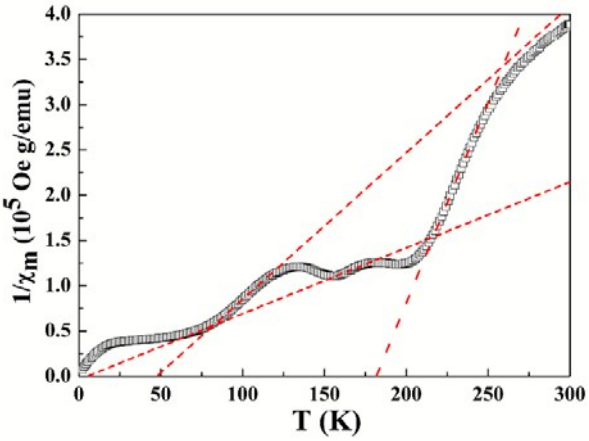

Fig. 5. Temperature dependence of inverse magnetic susceptibility in BFCT25. Two ferromagnetic Curie temperatures (50 K and 160 K) are obtained by fitting the linear parts of the curve with Curie-Weiss law χm = C/(T – Tc).

1.868 μ_B atom^{-1}, respectively), while their surrounding O atoms have a small contribution (less than 0.1μ_B/atom). A close inspection of the density of states reveals that the Fe d_{xy} orbital hybridizes with the Co d_{z^2} through the O p_y/p_z orbital and gives rise to ferromagnetic exchange coupling between adjacent Fe^{3+} and Co^{3+} ions (cf. Figure 5a). For Fe^{3+}-O-Fe^{3+} and Co^{3+}-O-Co^{3+} interactions with the typical Hubbard *U*, the exchange couplings were shown to be dominated by the (virtual) electron transfer between either an empty or fully-filled *d*-orbital and a half-filled *d*-orbital (*cf*. Table S4), which are ferromagnetic, consistent with the semi-empirical Goodenough-Kanamori rules. Therefore, in principle, the exchange interactions favour ferromagnetically ordered Fe/Co-rich regions in BFCT25, with nearest-neighbour Fe^{3+}-O-Fe^{3+}, Fe^{3+}-O-Co^{3+} and Co^{3+}-O-Co^{3+} ferromagnetic

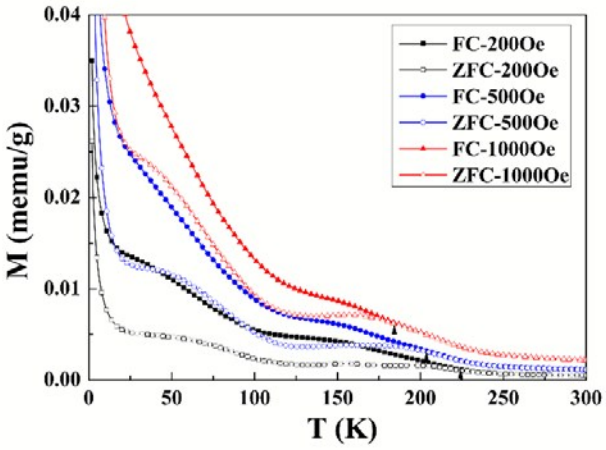

Fig. 6. Field cooled (FC) and zero field cooled (ZFC) magnetization curves of BFCT25 measured under different magnetic fields.

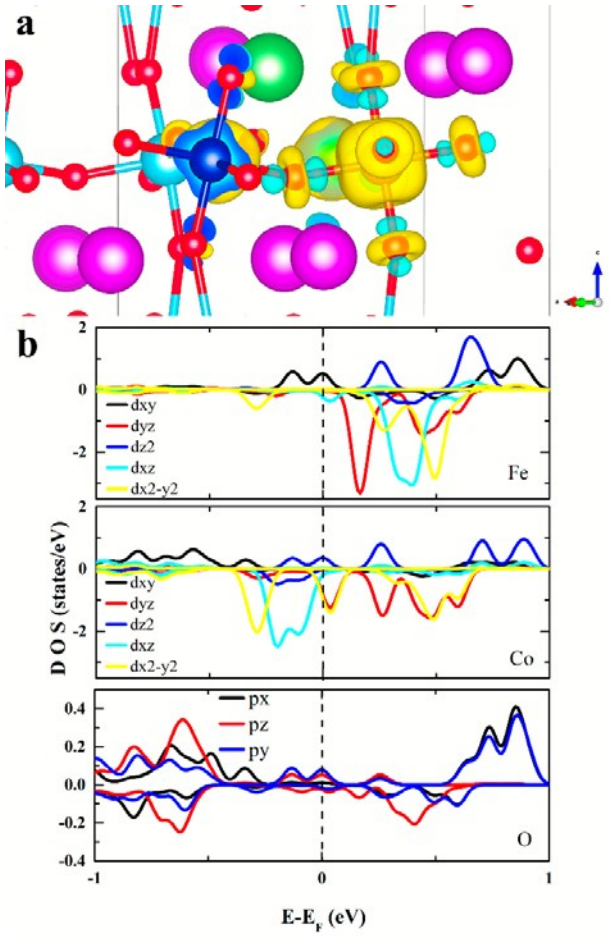

Figure 7. (a) Spin density of BFCT25 around O (red), Bi (pink), La (green), Ti (light blue), Co (dark blue) and Fe (yellow) atoms, and (b) density of states in BFCT25.

couplings of around 16.38 meV, 29.09 meV and 59.89 meV, respectively. These could be expected to give rise to the three ferromagnetic transitions in BFCT25, as observed experimentally.

Magnetoelectric Coupling

Given that the magnetic Fe^{3+}/Co^{3+} ions are responsible for the magnetism and also partly for the ferroelectricity of BFCT25, the regions with higher local concentrations of Fe^{3+}/Co^{3+} ions are expected to be multiferroic. These Fe/Co rich regions, randomly distributed in BFCT25, should exhibit an electrical response sensitive to an applied magnetic field such as observed in magnetoelectric multiferroics. In order to confirm the existence of ME coupling in the sample at room temperature, changes in the ferroelectric domain structure were investigated using piezoresponse force microscopy (PFM) under an in-plane magnetic field (Figure 8). The measurements were carried out on BFCT25 perpendicular to the SPS pressure direction (the microstructure image is presented in Figure S2). After applying a positive and then a negative magnetic field parallel to the sample surface (Figure 8b and 8c), the direction of the ferroelectric polarization in the highlighted areas rotates towards the out of plane direction. The contrast differences

View Article Online
DOI: 10.1039/C8TC00161H

observed in the PFM magnitude and in the phase signals provide evidence for the changes in ferroelectric polarization. Similar magnetic field-induced changes of FE polarization were previously observed in ceramic composites using PFM[24,44], but never in single-phase ceramics at room temperature. In Figure 6, the regions that experience the magnetic field-driven change in polarization are about 100-200 nm and are multiferroic. It is worth mentioning that the observed magnetoelectric behaviour has been rarely reported in truly single-phase materials at room temperature.

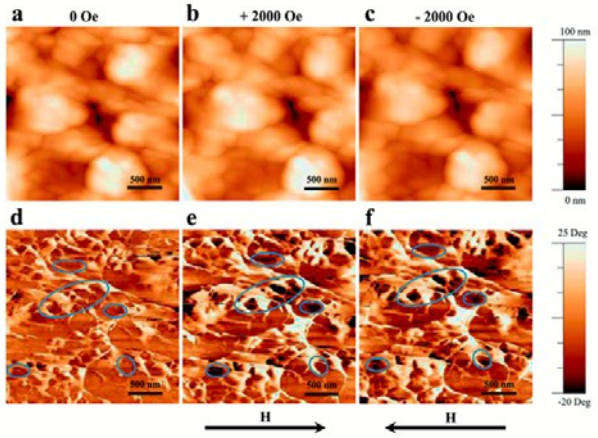

Figure 8. Ferroelectric domain switching under magnetic field in BFCT25. (a) Topography and (d) vertical PFM phase at zero magnetic field; (b) topography and (e) vertical PFM phase at +2000 Oe; (c) topography and (f) vertical PFM phase at -2000 Oe.

The presence of magnetoelectric coupling in BFCT25 was further confirmed by measurement of the magnetoelectric coupling coefficient (α_{ME}) at 100 K (Figure 9). A maximum value of α_{ME} was about 0.57 mV cm^{-1} Oe^{-1} at 2700 Oe.

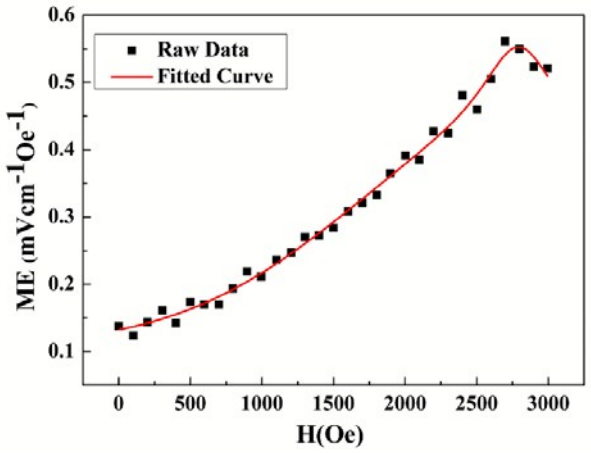

Fig. 9. Magnetoelectric coefficient (ME) of BFCT25 measured at 100 K through the measurement of magnetic field induced electric field. The value of maximum ME coefficient is 0.57 mV cm^{-1}Oe^{-1}.

Conclusions

The structural, electrical (dielectric and ferroelectric), magnetic and magnetoelectric properties of dense, grain-oriented $Bi_{3.25}La_{0.75}Ti_{3-2x}Nb_x(Fe_{0.5}Co_{0.5})_xO_{12}$ (x = 0.05, 025 and 0.35) ceramics were investigated. It was found that the solid solution limit in the system lies between x = 0.25 and 0.35. The x = 0.05 and 0.25 compositions exhibit a single-phase Aurivillius structure with orthorhombic symmetry in space group *B*2*cb*. The ferroelectric-paraelectric phase transition shifts toward lower temperatures with the increasing Fe/Co content. Lanthanum ions were found only at the A sites of the perovskite slabs, sharing this site with bismuth ions. The stereochemical activity of the Bi 6s^2 lone pair of electrons in the perovskite A-site and also in the bismuthate layer was evidenced by the X-ray and neutron diffraction studies. Weak ferromagnetism, originating from the exchange interaction between the Fe and Co spins, was confirmed to exist in the x = 0.25 sample by electron spin resonance measurements at room temperature. The results of first principles calculations confirm ferromagnetic coupling between the Fe^{3+} and Co^{3+} cations through oxygen atoms. Piezoresponse force microscopy revealed that the ferromagnetism in BFCT25 most likely originates from the Fe/Co rich regions of 100-200 nm in size. Changes observed in the ferroelectric domain structure upon the application of an external magnetic field imply multiferroic behaviour in the single-phase BFCT25 at room temperature. The discovery of the room temperature multiferroicity in this single-phase ceramic is expected to pave the way for achieving desired multiferroic properties via composition modification for different applications such as low energy consumption memory devices and sensors.

Conflicts of interest

There are no conflicts to declare.

Acknowledgements

This study was supported by the Royal Academy of Engineering Distinguished Visiting Fellowship, the Grant Agency of the Slovak Academy of Sciences (Grant No. 2/0059/17), CSS (Grant No. YK2015-0602006), NSFC (Grant No. 11474138), and PCSIRT (Grant No. IRT16R35).

Notes and references

1. N. Hur, S. Park, P. Sharma, J. Ahn, S. Guha and S. Cheong, *Nature*, 2004, **429**, 392-395.
2. J. Shah and R. Kotnala, *Journal of Materials Chemistry A*, 2013, **1**, 8601-8608.
3. M. Trassin, *Journal of Physics: Condensed Matter*, 2016, **28**, 033001.
4. T. Onuta, Y. Wang, C. J. Long, and I. Takeuchi, *Applied Physics Letters*, 2011, **99**, 203506.
5. S. R. Etesami and J. Berakdar, *Applied Physics Letters,* 2016, **108**, 053903.
6. R. Gupta, M. Tomar, A. Kumar and V. Gupta, *Smart Materials and Structures*, 2017, **26**, 035002.

View Article Online
DOI: 10.1039/C8TC00161H

7. D. Takashima and I. Kunishima, *IEEE Journal of Solid-State Circuits*, 1998, **33**, 787-792.
8. A. P. Pyatakov and A. K. Zvezdin, *Physics-Uspekhi*, 2012, **55**, 557-581.
9. M. Vopsaroiu, J. Blackburn, A. Muniz-Piniella and M. G. Cain, *Journal of Applied Physics*, 2008, **103**, 07F506.
10. N. A. Hill, *The Journal of Physical Chemistry B*, 2000, **104**, 6694-6709.
11. T. Kimura, Y. Sekio, H. Nakamura, T. Siegrist and A. Ramirez, *Nature materials*, 2008, **7**, 291-294.
12. T. Kimura, T. Goto, H. Shintani, K. Ishizaka, T. Arima and Y. Tokura, *Nature*, 2003, **426**, 55-58.
13. J. A. Mundy, C. M. Brooks, M. E. Holtz, J. A. Moyer, H. Das, A. F. Rébola, J. T. Heron, J. D. Clarkson, S. M. Disseler and Z. Liu, *Nature*, 2016, **537**, 523-527.
14. S. Dong, J. Liu, S. Cheong and Z Ren, *Adv. Phys*, 2015, 64, 519-629.
15. M. Palizdar, T. P. Comyn, M. B. Ward, A. P. Brown, J. P. Harrington, S. Kulkarni, L. Keeney, S. Roy, M. Pemble, R. Whatmore, C. Quinn, S. H. Kilcoyne and A. J. Bell, *Journal of Applied Physics*, 2012, **112**, 073919.
16. N. A. Spaldin, S.-W. Cheong and R. Ramesh, *Physics Today*, 2010, **63**, 38-43.
17. G. Catalan and J. F. Scott, *Advanced materials*, 2009, **21**, 2463-2485.
18. M. Fiebig, *Journal of Physics D: Applied Physics*, 2005, **38**, R123.
19. R. Turner, P. A. Fuierer, R. Newnham and T. Shrout, *Applied Acoustics*, 1994, **41**, 299-324.
20. X. Mao, W. Wang, X. Chen and Y. Lu, *Applied Physics Letters*, 2009, **95**, 082901.
21. L. Keeney, T. Maity, M. Schmidt, A. Amann, N. Deepak, N. Petkov, S. Roy, M. E. Pemble, R. W. Whatmore and D. Johnson, *Journal of the American Ceramic Society*, 2013, **96**, 2339-2357.
22. A. Faraz, T. Maity, M. Schmidt, N. Deepak, S. Roy, M. E. Pemble, R. W. Whatmore and L. Keeney, *Journal of the American Ceramic Society*, 2017, **100**, 975-987.
23. Z. Shen, J. Liu, J. Grins, M. Nygren, P. Wang, Y. Kan, H. Yan and U. Sutter, *Advanced materials*, 2005, **17**, 676-680.
24. H. Yan, H. Zhang, R. Ubic, M. J. Reece, J. Liu, Z. Shen and Z. Zhang, *Advanced materials*, 2005, **17**, 1261-1265.
25. R. Newnham, R. Wolfe and J. Dorrian, *Materials Research Bulletin*, 1971, **6**, 1029-1039.
26. A. Srinivas, S. Suryanarayana, G. Kumar and M. M. Kumar, *Journal of Physics: Condensed Matter*, 1999, **11**, 3335.
27. Z. Li, J. Ma, Z. Gao, G. Viola, V. Koval, A. Mahajan, X. Li, C. Jia, C. Nan and H. Yan, *Dalton Transactions*, 2016, **45**, 14049-14052.
28. J. Liu, Z. Shen, H. Yan, M. J. Reece, Y. Kan and P. Wang, *Journal of Applied Physics*, 2007, **102**, 682.
29. U. Chon, H. M. Jang, M. Kim and C. Chang, *Physical review letters*, 2002, **89**, 087601.
30. H. S. Shulman, M. Testorf, D. Damjanovic and N. Setter, *Journal of the American Ceramic Society*, 1996, **79**, 3124-3128.
31. A. C. Larson and R. Von Dreele, *Los Alamos National Laboratory Report No*, LA-UR-86-748, 1987.
32. S.-J. Oh, Y. Shin, T. T. Tran, D. W. Lee, A. Yoon, P. S. Halasyamani and K. M. Ok, *Inorganic chemistry*, 2012, **51**, 10402-10407.
33. K. Momma and F. Izumi, *Journal of Applied Crystallography*, 2011, **44**, 1272-1276.
34. G. Viola, T. Saunders, X. Wei, K. B. Chong, H. Luo, M. J. Reece and H. Yan, *Journal of Advanced Dielectrics*, 2013, **03**, 1350007.
35. M. Mahesh Kumar, A. Srinivas, S. Suryanarayana, G. Kumar and T. Bhimasankaram, *Bulletin of Materials Science*, 1998, **21**, 251-255.
36. J. B. Neaton, C. Ederer, U. V. Waghmare, N. A. Spaldin and K. M. Rabe, *Physical Review B*, 2005, **71**, 4113.
37. A. Y. Birenbaum and C. Ederer, *Physical Review B*, 2014, **90**, 214109.
38. K. Knížek, Z. Jirák, J. Hejtmánek, P. Novák and W. Ku, *Physical Review B Condensed Matter*, 2009, **79**, 014430.
39. J. Cumby and J. P. Attfield, *Nature Communications*, 2017, **8,** 14235.
40. N. C. Hyatt, J. A. Hriljac and T. P. Comyn, *Materials research bulletin*, 2003, **38**, 837-846.
41. H. Yan, F. Inam, G. Viola, H. Ning, H. Zhang, Q. Jiang, T. A. O. Zeng, Z. Gao and M. J. Reece, *Journal of Advanced Dielectrics*, 2011, **01**, 107-118.
42. Y. Shimakawa, Y. Kubo, Y. Nakagawa, S. Goto, T. Kamiyama, H. Asano and F. Izumi, *Physical Review B*, 2000, **61**, 6559.
43. H. Zhao, H. Kimura, Z. Cheng, M. Osada, J. Wang, X. Wang, S. Dou, Y. Liu, J. Yu and T. Matsumoto, *Scientific Reports*, 2014, **4**, 5255.
44. L. F. Henrichs, O. Cespedes, J. Bennett, J. Landers, S. Salamon, C. Heuser, T. Hansen, T. Helbig, O. Gutfleisch, D. C. Lupascu, H. Wende, W. Kleemann and A. J. Bell, *Advanced Functional Materials*, 2016, **26**, 2111-2121.